Materials Advances

ROYAL SOCIETY OF CHEMISTRY

PAPER

View Article Online
View Journal | View Issue

Cite this: *Mater. Adv.*, 2022, 3, 3326

Aggregate dependent electrochromic properties of amino acid appended naphthalene diimides in water†

Rebecca I. Randle, [a] Leide Cavalcanti,[b] Stephen Sproules [a] and Emily R. Draper *[a]

Received 22nd February 2022,
Accepted 11th March 2022

DOI: 10.1039/d2ma00207h

rsc.li/materials-advances

Naphthalene diimides can have electrochromic applications due to their highly stable dark reduced state along with a transparent colourless neutral state. We show here that the colouration and reversibility of water-dispersible amino acid appended NDIs are directly influenced by the aggregated state present at different pH using spectroelectrochemistry, small angle neutron scattering (SANS) and cyclic voltammetry (CV). We find the aggregation itself is influenced by both pH and the amino acid or dipeptide in the structure, with each NDI having a preferred morphology giving rise to a more intensely coloured state.

Introduction

Small organic electrochromic molecules are gaining focus.[1,2] Organic molecules can offer broad absorbance,[1] fast switching between coloured states,[3] often low cost and facile synthesis,[4] and high stability and variety of coloured states.[5] They seem a very attractive alternative to inorganics, which often are expensive,[6,7] can be toxic and can need high processing temperatures due to metals contained within them. Not only is this energetically expensive, but it can be highly damaging to the environment.[8–10] In order to be developed on an industrial scale, materials should be soluble in environmentally friendly, non-toxic solvents. Water is an attractive solvent when considering material practicality with solubility being one the most important factors. Many organic materials are poorly soluble in water unless specially functionalised. Viologens currently dominate the class of organic electrochromics[11–13] due to their intense colouration. However, they often perform poorly in aqueous solution due to side reactions and recrystallisation but can be functionalised to be soluble.[14] Naphthalene diimides (NDIs) have high colouration with fast switching times,[15–17] tunability through low-cost synthesis and low toxicity.[17] Critically NDIs also can self-assemble in water. These assemblies can then be influenced easily by functional group or environment (*i.e.* using pH or concentration, much like a surfactant).[16,18] In other related fields this self-assembly has been taken advantage of to modify material properties such as, mechanical strength, photoconductivity and catalytic activity.[19–22] Self-assembly behaviour can be tuned without changing the chemical structure, just by altering assembly conditions, something unachievable with single molecules, which in turn can give otherwise unattainable structures and architectures.[19–22] This is a huge advantage, as new molecules do not need to be designed, synthesised and characterised, and we can rather focus on teaching a known molecule new tricks. Prediction of colour, stability and switching times is currently almost impossible; overcoming this, and therefore could save valuable time and resources. NDIs are known to form one-dimensional π dimers and stacks[23] which then fold or assembles into larger assemblies[24] such as spheres or cylinders. However, these different assemblies have not yet been fully explored within this area of electrochromics.

Here, we examine the effect of self-assembled structure on electrochromic properties by looking at five different water-soluble NDIs. The NDIs we use here have two free carboxylic acids (Fig. 1). The absolute chemical structure influences the apparent pK_a, and so pH can be used to tailor the state of these systems by having both, one, or none of the carboxylic acids in their protonated states.[19–21]

The level of protonation effects the solubility of the molecule and drives the assembly. Indeed, in our previous study on an electrochromic window, we noted **NDI-GF** (NDI appended with glycine–phenylalanine, Fig. 2) in a water/glycerol solvent mix, behaved differently in the window systems above and below the molecule's apparent pK_a, with little or no structure at high pH and fibrous gelled network at low pH.[17] In this study, we show

[a] *School of Chemistry, JBB University of Glasgow, Glasgow, G12 8QQ, UK. E-mail: emily.draper@glasgow.ac.uk*
[b] *ISIS Neutron and Muon Source User Office, Science and Technology Facilities Council, Rutherford Appleton Laboratory, Harwell Oxford, Didcot, OX11 0QX, UK*

† Electronic supplementary information (ESI) available. See DOI: 10.1039/d2ma00207h

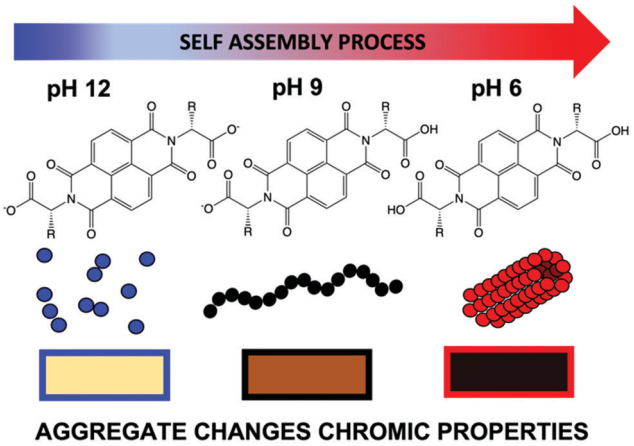

Fig. 1 Cartoon showing how an example NDI can have different aggregations depending on pH, ultimately effecting the colour of the reduced species in water.

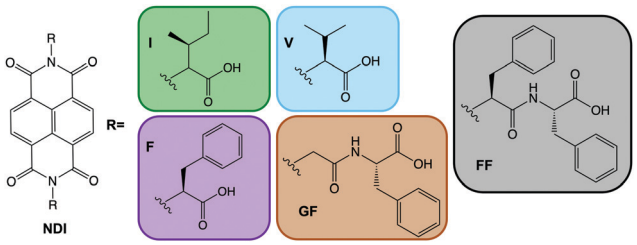

Fig. 2 Chemical structures of **NDI-I**, **NDI-V**, **NDI-F**, **NDI-GF** and **NDI-FF**.

that NDIs have different colouration depending on the conditions under which they are assembled. A colourless state is seen in neutral conditions and a deeply coloured state upon electrochemical reduction, an advantage compared to other systems which require continuous energy for both states.[25] By understanding the influence of chemical structure, pH and aggregate formed on the properties we can tailor these systems for electrochromic application.

Results and discussion

Our systems have two apparent pK_a values that differ slightly depending on R and are in the range of pH 9.2–9.6 and pH 6.4–6.8 (Fig. S39–S43 and Table S6, ESI†). We therefore examined each of the NDIs above both pK_a values (pH 12), at the highest pK_a (pH 9) and at the lowest pK_a (pH 6). We expect aggregation to change at these points with a general trend that as pH lowers, aggregates are likely to get larger, as for other similar systems.[17] First the absorptions of the neutral and electrochemically reduced and oxidised states were measured. At pH 12, the neutral state of all NDIs show a broad peak around 340–380 nm (Fig. 3 and Fig. S44–S47, ESI†) suggesting a similar aggregated state present in all the systems. **NDI-FF** however had an extra peak 310 nm suggesting a different aggregation to the others (Fig. 3(b) and Fig. S48, ESI†).

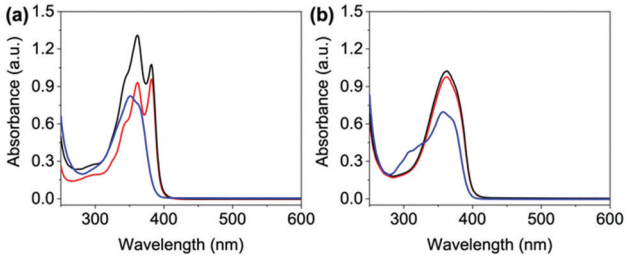

Fig. 3 Absorbance spectra of neutral states of (a) **NDI-GF** and (b) **NDI-FF**. Solutions adjusted to pH 6 (—), 9 (—) and 12 (—).

On applying a potential of −2.5 V, at pH 12, there is little reduction in all the NDIs seen in the absorption spectra, and therefore no colour change by eye (blue data Fig. 4 and Fig. S49–S52, ESI†) and have slow oxidation rates (Fig. S53–S57, ESI†). At pH 6 and 9 the neutral absorption spectra of **NDI-I**, **NDI-V**, **NDI-F** and **NDI-GF** are comparable in terms of peak positions, with defined peaks at 365 and 385 nm and a small shoulder at 345 nm (Fig. S44–S47, ESI†). The spectra of **NDI-FF** again are notably different (Fig. S48, ESI†), with a broad absorbance being observed at 360 nm. The ratio of peaks in the absorption spectra are comparable at pH 6 and 9 with the exception of **NDI-GF** where this ratio is observed to change between pH 6 and 9, suggesting a subtle change in molecular packing (Fig. 3(a) and Fig. S47, ESI†). While there is no real difference observed in the neutral spectra of other NDIs at pH 6 and 9, there is a significant difference in the intensity in their reduced states (Fig. 4 and Fig. S49–S52, ESI†). This difference was most significant in **NDI-I** and **NDI-V**, both being darkest at pH 9 by eye and in intensity in the absorption spectra (Fig. S49 and S50, ESI†). The reduced states of **NDI-GF**, **NDI-F** and **NDI-FF** are instead more intense in colour at pH 6 (Fig. 4 and Fig. S51 and S52, ESI†). The molar extinction coefficients are shown in Table S7 (ESI†), but there is no observed trend between them and colouration intensity, for example **NDI-V**

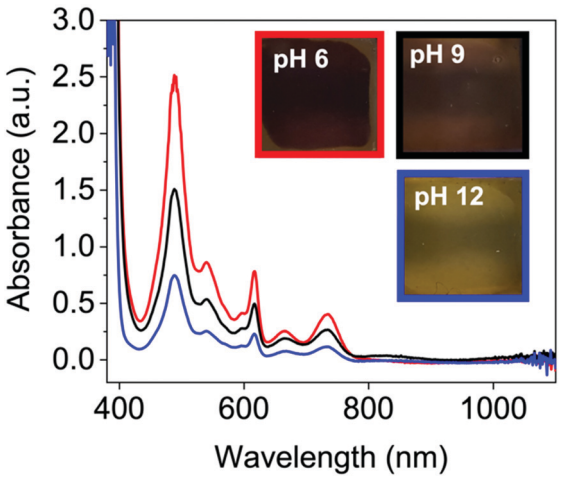

Fig. 4 Reduced absorbance spectra of **NDI-F** solution at pH 6 (—), 9 (—) and 12 (—). Inset images of the resulting colouration are shown at pH 6, red square, pH 9 black square and pH 12, blue square.

and **NDI-FF** have comparable values yet show different coloration intensity. This suggests that the chromic behaviour of the material is not inherently coming from the chemical structure, but rather from the aggregates formed at the different pHs. Further to this, the pH corresponding to the darkest colouration upon reduction was also found to have the fastest electrochemical oxidation speed from a reduced state (Fig. S53–S57, ESI†). Therefore, there is an 'ideal' aggregated state and pH for these NDIs. For **NDI-V** and **NDI-I** this is pH 9, and for **NDI-GF** and **NDI-F** this is pH 6. More discussion about buffering is available in Section S3.1, Fig. S58–S73 and Tables S8, S9 (ESI†).

To further understand the differences in performance, we moved to SANS and viscosity to assess the structures present in solution. We examined each NDI at their 'ideal' pH (**NDI-GF**, **NDI-F** and **NDI-FF** at pH 6 and **NDI-I** and **NDI-V** at pH 9) and the poorest condition (pH 12 in all cases). The viscosity and SANS data suggested worm-like micelles were present in solution at the 'ideal' pH (Fig. S74 and Section S3.2, ESI†) and then less structured aggregates or fewer aggregates at pH 12, agreeing with our hypothesis of specific aggregation state being needed for the colouration.[26–28] The SANS data at the 'ideal' pD (measurements in D_2O needed for contrast) suggests that **NDI-I** and **NDI-V** form comparable structures to each other (Fig. 5(a) and Fig. S75, S76, ESI†). The data fit best to a flexible cylinder model combined with a power law. The length of these cylinders is outside the range accessible by this technique, but the radius of these cylinders is approximately 5 Å and they have a Kuhn length of approximately 118 and 111 Å for **NDI-I** and **NDI-V** respectively (Tables S10 and S11, ESI†). The scattering data for **NDI-GF** fit best to a flexible elliptical cylinder model whereas the data for **NDI-F** fit to a hollow cylinder model, both combined with a power law (Fig. S77, S78 and Tables S12, S13, ESI†). **NDI-F** has a lower scattering intensity than the other measured NDIs (Fig. 5), which suggests that it is made up of smaller, or more solvated aggregates. Both **NDI-F** and **NDI-GF** have larger radii than **NDI-I** and **NDI-V**. **NDI-GF** shows a high scattering intensity at low Q which suggests that there are larger, more complex structures in solution (Fig. 5).

At their 'ideal' pD, there is no commonality in model or scattering intensity that covers all NDIs, but at pH 12 there is (Fig. 5(b) and Fig. S79, ESI†). SANS data for all NDIs measured at pD 12 can be fit to a flexible elliptical cylinder models combined with a power law. The radius is approximately 5 Å and the ratio axis is very large (Fig. S80–S83 and Tables S14–S17, ESI†). This large axis ratio could suggest that the cylinders are not fully formed at high pH or that the structures are more similar to tapes.[29] Regardless of chemical structure, at pD 12, all NDIs measured with SANS scattered with almost identical intensity across all ranges of Q (Fig. 5(b)). More discussion of the NDIs at their 'non-ideal' pD can be found in the Section S3.3, Fig. S79–S87 and Tables S14–S21 (ESI†). The scattering for **NDI-FF** at its 'ideal' pD *vs.* pD 12 were comparable to each other, Fig. 5(b), suggesting the poor chromic behaviour observed is due to an unfavourable aggregation (more discussion in Section S3.4, Fig. S89–S91 and Tables S22, S23, ESI†).

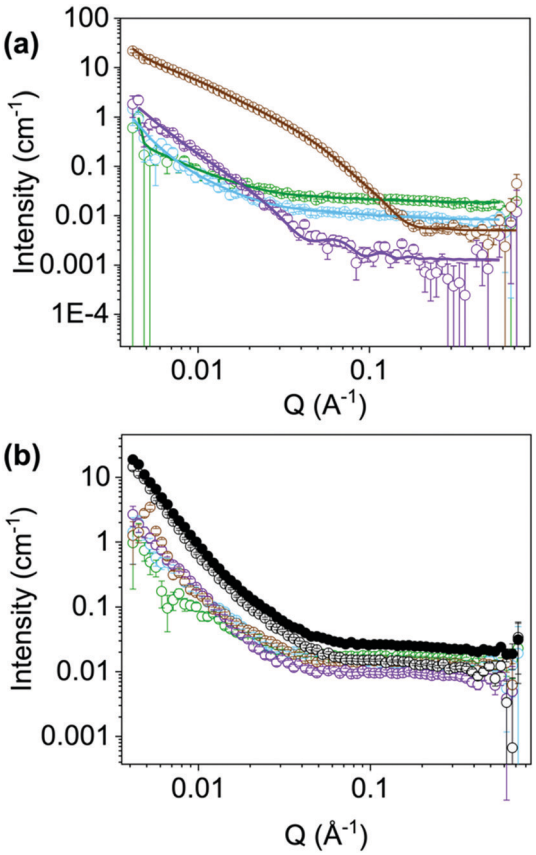

Fig. 5 (a) SANS (open circles) and fits (lines) solutions of **NDI-I** (—), **NDI-V** (—), **NDI-F** (—) and **NDI-GF** (—) at their 'ideal' pD (b) SANS (open circles) of solutions of **NDI-I** (—), **NDI-V** (—), **NDI-F** (—), **NDI-GF** (—) and **NDI-FF** (—) at pD 12 and **NDI-FF** (—) at its ideal pD (filled circles).

The SANS data may suggest that in the case of **NDI-I** and **NDI-V** that more rigid flexible cylinders support their chromic behaviour. Whereas **NDI-F** and **NDI-GF** data suggest that larger aggregates at lower pD support their chromic properties.

It appears that NDIs with aromatic R groups demonstrate a different 'ideal' pH to those with aliphatic groups but we believe that structure and larger aggregates present are the key cause of observed changes in electrochromic properties. In particular, the bulky, hydrophobic nature of the of **NDI-FF** may hinder the formation of long cylindrical aggregates and may also hinder π stacking (which in turn affects larger aggregation), making it unable to stabilise the radical needed for the colour change. The fibrous and more rigid aggregates formed at pH 6 and 9 for the NDIs and not at pH 12 aid radical stabilisation. NDI systems have been reported to have improved charge carrier transport upon formation of the radical anionic species when fibrous networks can form due to increased hydrogen bonding.[30] Similarly, we would expect aggregation of these species to affect efficiency of electron transfer and efficiency of redox processes as well as the stability of the radical anion. It is difficult to directly link chemical structure to behaviour in the aggregated state, as many properties change at the same time, like hydrophobicity, molecular weight,

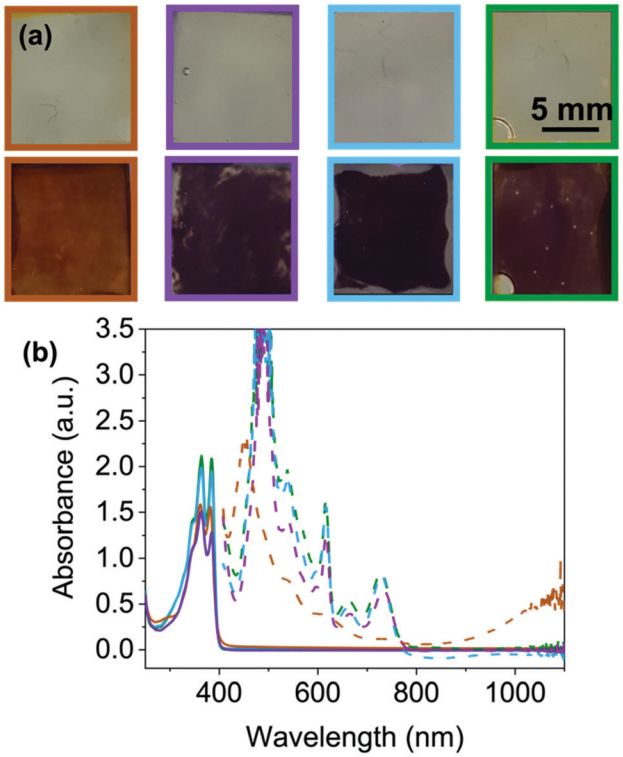

Fig. 6 (a) Photographs of **NDI-I** (—), **NDI-V** (—) adjusted to pH 9 and **NDI-F** (—) and **NDI-GF** (—) adjusted to pH 6 in their neutral (top) and reduced states (bottom) (b) absorbance spectra of same solutions in neutral (solid line) and reduced (dashed line) state. Because of absorbance from FTO glass over 400 nm, this section of the data is removed. Intensity of absorbance at 485 nm is too large for the spectrometer.

intermolecular bonding and pK_a. For our systems, we believe it is a combination of factors, which is overall driven by the aggregate type that is causing the differences in behaviour between the NDIs.

To further determine stability and depth of colour we then moved to FTO windows (see ESI† for full set up details) for the four NDIs that showed a colour change. As mentioned previously, there is little difference between the neutral NDIs in the position of the absorbance peaks at their 'ideal' pH (Fig. 6(b) and Fig. S92, ESI†). Each show two peaks of equal intensity, apart from **NDI-F**, where the peak at 385 nm is significantly reduced compared to 365 nm, suggesting a small difference in molecular packing compared to the other NDIs. However, by eye this difference cannot be seen, and all appear to be colourless and transmissive in the neutral state (Fig. 6 top).

Where the NDIs do differ is in the colouration achieved by these systems upon reduction. **NDI-I**, **NDI-V** and **NDI-F** show a darker more purple colouration, whereas **NDI-GF** appears brown/black when electrochemically reduced (Fig. 6(a) bottom). These colours have been reported to be characteristic of the NDI dianion or radical anion respectively,[15] however, other reported systems observed report orange and pink.[31] EPR spectroscopy suggests that radical anions (Fig. S93–S97 and Section S3.5, ESI†) are comparable between the NDIs. The EPR signal from **NDI-GF** has lower symmetry than that produced by other NDIs (Fig. S97, ESI†). **NDI-I**, **NDI-V**, **NDI-F** and **NDI-FF** produce similar signals to each other, with subtle differences in hyperfine coupling which could be due to molecular motion rather than inherent electronic differences. Therefore, we again attribute colouration to differences in the ability of the aggregated structure to stabilise the radical or form the dianion rather than from being different radicals.

For reduced **NDI-I** and **NDI-V** there is a characteristic dianion peak around 410–415 nm[15,17] (Fig. 6(b) and Fig. S98, ESI†). No dianion peak is observed in the spectrum of **NDI-F** and the colour is comparable to **NDI-I** and **NDI-V**. We hypothesise that **NDI-I** and **NDI-V** aggregates can stabilise the dianion better than the other NDIs, but the radical anion is the majority species in solution due to the large EPR signal and very dark colour which dominates. Reduced spectra of **NDI-GF** are notably different (Fig. 6(b) and Fig. S98, ESI†). In the reduced solutions of **NDI-GF**, a broad absorption in the near IR region over 900 nm is associated with one-dimension π-stacking of the radical anion.[15,17,23] This observation suggests different packing to the other NDIs, resulting in a different colouration, the lower symmetry in the EPR spectrum also supports **NDI-GF** behaving differently to the other NDIs. The colouration efficiency and transmittance of states are discussed in Section S3.6 and Table S24 (ESI†).

To look at switching speeds and stability of the reduced states, we used CV and spectroelectrochemistry. A reduction potential of −2.5 V and an oxidation potential of 0.2 V were used for the switching between the two states (Fig. 7(a) and Table S25, Fig. S99 (ESI†), a full discussion about these procedures can be found in the Section S3.6, Fig. S100–S109 and Tables S26–S29, ESI†). For each of the materials, the reduction potential is only needed for a few seconds to achieve the darkest colouration. However, in this set up, an oxidising potential of least a minute is required to remove the radical and colour, Fig. 7(a) and Fig. S58–S61 (ESI†), with **NDI-I** and **NDI-F** showing the fastest oxidation, Fig. 7(a). This could be due to the oxidation being energetically more difficult to achieve, diffusion of the aggregates away from electrode surfaces or the aggregates themselves stabilising and effectively shielding the radical from oxidation as seen in other systems.

Upon 100 redox cycles, the current of the oxidation peak decreases for **NDI-V** and **NDI-GF** while increasing in **NDI-I** and remaining consistent in **NDI-F** (Fig. S110–S113, ESI†). This observation suggests that resistivity is higher after 100 cycles in **NDI-V** and **NDI-GF** which makes oxidation less viable. The decrease in oxidation is most significant in **NDI-GF** (the peak becoming less visible over time, Fig. S113, ESI†). The potentials of **NDI-V** shift the most over cycles (Fig. S111, ESI†). Both these factors could have implications for long term cyclability. There is also a reduction in current over the cycles for the reduction process, with the largest change seen for **NDI-GF** (Fig. S113, ESI†). This change may be due to the increasing amount of radical anion present at the electrode surface with each scan, so the proportion of neutral species available to reduce decreases or could again be due to diffusion of material away from the electrode surface. It is clear here that aggregate has an effect

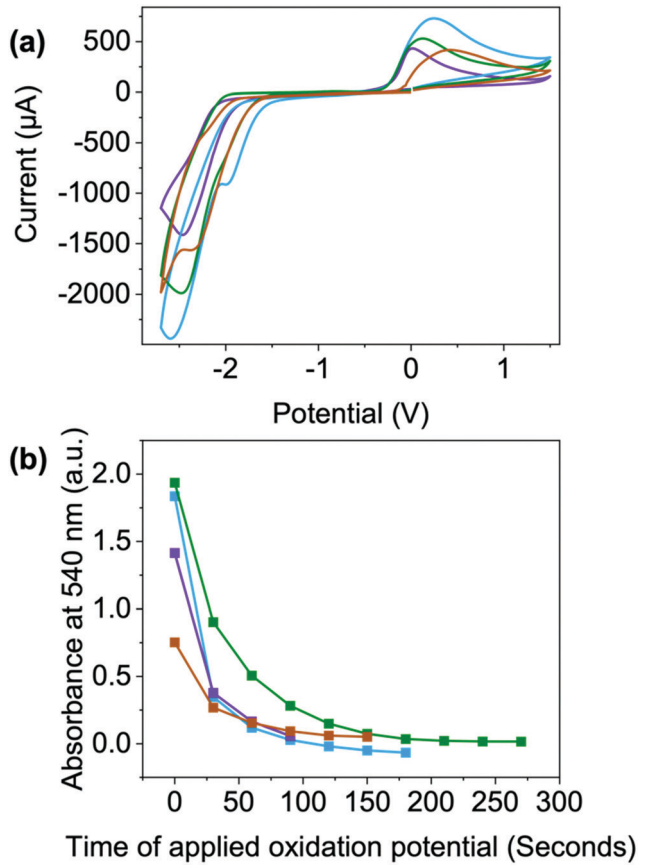

Fig. 7 (a) Cyclic voltammograms collected from buffered 10 mg mL^{-1} solutions of **NDI-I** (—), **NDI-V** (—) adjusted to pH 9 and **NDI-F** (—) and **NDI-GF** (—) adjusted to pH 6 voltammograms measured in 1 × 1 cm FTO windows. The scan rate of the cyclic voltammograms was 0.1 V s^{-1}. (b) Time taken after the application of the oxidising potential for the absorption at 540 nm to return to 0.

here also, either it be due to diffusion or their ability to stabilise or shield the radical, rather than electronic differences arising from chemical structure. While there may be other factors such as electron transfer which affect the electrochemical processes, aggregation here has a large impact on the electrochromic behaviour of these systems in depth of colour and switching times.

Experimental

Full experimental, methods and protocols can be found in the Section S1 of the ESI.† Further details on FTO windows, spectroelectrochemistry, cyclic voltammetry, viscosity, EPR, SANS, pK_a titrations, transmittance and UV-vis absorption can be found in Section S2 of the ESI.†

Synthetic procedures

Each NDI was synthesized in the reaction between naphthalene-1,4,5,8-tetracarboxylic acid dianhydride and the corresponding dipeptide or amino acid in molten imidazole following standard protocols. The full experimental details and characterization are available in the ESI.†

Materials and methods

Solutions were prepared at concentrations 10 mg mL^{-1} of NDI (unless otherwise stated). NDI solids were dissolved in 2 molar equivalents of aqueous NaOH (0.1 M) and 400 μL mL^{-1} of 0.1 M NaCl (to act as a background electrolyte). The remaining volume of solutions were made up with deionised water. This concentration was chosen due to the intensity of colour produced upon electrochemical reduction. As shown in Fig. S26–S30 (ESI†), the structures dilute upon decreasing concentration rather than change aggregation state. Solutions were stirred overnight until all solids had dissolved. Solutions were adjusted between pH 6–12 in increments of 1 unit. However, only pH 6, 9 and 12 are shown in the main article as this is where changes in aggregation occur.

UV-vis absorption spectroscopy

Absorption spectra were collected using a Cary 60 UV-Visible spectrophotometer from Agilent Technologies. Solutions were measured in a 0.1 mm pathlength quartz cuvette (Hellma Analytics) or spectro-electrochemical cells (BASi). Spectra were collected from 250–1100 nm at a scan rate of 2 nm s^{-1} unless stated otherwise.

Small angle neutrons scattering

Solutions were prepared as previously described but using deuterated solvent and base. The measurements were performed using the SANS2D instrument (STFC ISIS Pulsed Neutron Source, Oxfordshire, UK) by Dr Leide Cavalcanti. A multiple-slot sample changer with controlled temperature of 25 °C was used. The beamline setup was 4 m sample-to-detector distance, beam size of 8 mm and a typical Q-range [$Q = 4\pi \sin(\theta/2)/\lambda$, where q is the scattering angle] from 0.004 Å^{-1} to 0.7 Å^{-1} set by time-of-flight mode with incident wavelengths (l) from 1.75 Å to 16.5 Å. Samples were placed in 2 mm quartz cuvettes and measured for ~60 minutes. The scattering data were normalized for the sample transmission and background corrected D_2O data reduction was performed using Mantid framework15 installed inside the ISIS virtual machines, IDAaaS.

Behaviour in windows

Solutions were deposited (<0.2 mL) and secured in FTO window cells and a potential of −2.5 V applied for 10 seconds. These values were used based on cyclic voltammograms (Fig. S34–S38 and Tables S1–S5, ESI†). Functional group impacts the position of the oxidation potential, assessed by cyclic voltammetry, but not significantly. All values are within a 0.4 V window and so the reduction and oxidation potential were kept consistent through all measurements. The absorbance spectra were then collected immediately after reduction. Photographs were taken after a 10 second application of −2.5 V on a separate occasion with the cell outside of the spectrometer for ease (Fig. 4 and Fig. S49–S52, ESI†).

Conclusions

In summary, we show that NDIs exhibit different electrochromic properties, that would not be obvious from their chemical structure alone. Our work here demonstrates the power in tuning the aggregation of a single molecule alone in water just by changing pH, an exciting opportunity that organics have over inorganics, in a wide variety of electrochromic applications. More importantly, this work highlights that all these conditions should be thoroughly explored and tested before discounting organics for electrochromics.

Author contributions

R. R. – formal analysis, investigation. L. C. – investigation, data curation. S. S. – investigation, resources. E. R. D. – conceptualisation, funding acquisition, project administration, resources, supervision. All authors contributed to the writing of the manuscript.

Conflicts of interest

There are no conflicts to declare.

Acknowledgements

We thank the Leverhulme Trust (ECF-2017-223), the EPSRC (EP/S032673/1) and (EP/N509668/1), and the UKRI (MR/V021087/1) for funding. This work benefitted from SasView software, originally developed by the DANSE project under NSF award DMR-0520547.

Notes and references

1 R. J. Mortimer, *Electrochim. Acta*, 1999, **44**, 2971–2981.
2 T. A. Welsh and E. R. Draper, *RSC Adv.*, 2021, **11**, 5245–5264.
3 S. Abraham, S. Mangalath, D. Sasikumar and J. Joseph, *Chem. Mater.*, 2017, **29**, 22.
4 A. A. Argun, *et al.*, *Chem. Mater.*, 2004, **16**, 4401–4412.
5 H.-J. Yen, K.-Y. Lin and G.-S. Liou, *J. Mater. Chem.*, 2011, **21**, 6230–6237.
6 S. Xie, *et al.*, *Chem. – Eur. J.*, 2019, **370**, 1459–1466.
7 R. Baetens, B. Petter Jelle and A. Gustavsen, *Sol. Energy Mater. Sol. Cells*, 2009, **94**, 87–105.
8 G. A. Niklasson and C. G. Granqvist, *J. Mater. Chem.*, 2006, **17**, 127–156.
9 M. Kamalisarvestani, *et al.*, *Renewable Sustainable Energy Rev.*, 2013, **26**, 353–364.
10 C. G. Granqvist, *J. Vac. Sci. Technol., B*, 2014, **32**, 060801.
11 A. Donnadieu, *Mater. Sci. Eng., B*, 1989, **3**, 185–195.
12 Y. Alesanco, *et al.*, *Adv. Opt. Mater.*, 2017, **5**, 1600989.
13 K. Madasamy, *et al.*, *J. Mater. Chem.*, 2019, **4622**, 4622.
14 T. H. Chang, *et al.*, *Sol. Energy Mater. Sol. Cells*, 2018, **177**, 75–81.
15 G. Andric, *et al.*, *Aust. J. Chem.*, 2004, **57**, 1011–1019.
16 M. al Kobaisi, S. v. Bhosale, K. Latham, A. M. Raynor and S. v. Bhosale, *Chem. Rev.*, 2016, **116**, 11685–11796.
17 L. Gonzalez, C. Liu, B. Dietrich, H. Su, S. Sproules, H. Cui, D. Honecker, D. J. Adams and E. R. Draper, *Commun. Chem.*, 2018, **1**, 77.
18 S. V. Bhosale, C. H. Jani and S. J. Langford, *Chem. Soc. Rev.*, 2008, **37**, 331–342.
19 E. R. Draper, B. J. Greeves, M. Barrow, R. Schweins, M. A. Zwijnenburg and D. J. Adams, *Chem*, 2017, **2**, 716–731.
20 C. L. Smith, L. L. E. Mears, B. J. Greeves, E. R. Draper, J. Doutch, D. J. Adams and A. J. Cowan, *Phys. Chem. Chem. Phys.*, 2019, **21**, 26466–26476.
21 D. McDowall, *et al.*, *Adv. Energy Mater.*, 2020, **10**, 1–10.
22 E. R. Draper, *et al.*, *Chem. – Eur. J.*, 2018, **24**, 4006–4010.
23 K. R. Miller and L. L. Mann, *Acc. Chem. Res.*, 1996, **29**, 417–423.
24 H. Kar, R. Molla and S. Ghosh, *Chem. Commun.*, 2013, **49**, 4220.
25 A. Llordés, G. Garcia, J. Gazquez and D. J. Milliron, *Nature*, 2013, **500**, 323–326.
26 E. R. Draper, *et al.*, *Angew. Chem., Int. Ed.*, 2017, **56**, 10467–10470.
27 E. R. Draper, O. O. Mykhaylyk and D. J. Adams, *Chem. Commun.*, 2016, **52**, 6934–6937.
28 J. J. Walsh, J. R. Lee, E. R. Draper, S. M. King, F. Jä, M. A. Zwijnenburg, D. J. Adams and A. J. Cowan, *J. Phys. Chem. C*, 2016, **120**, 18479–18486.
29 J. C. MacDonald and G. M. Whitesides, *Chem. Rev.*, 1994, **94**, 2383–2420.
30 N. Nandi, S. Basak, S. Kirkham, I. W. Hamley and A. Banerjee, *Langmuir*, 2016, **32**, 13226–13233.
31 S. Guha and S. Saha, *J. Am. Chem. Soc.*, 2010, **132**, 17674–17677.